Decay-Associated Fluorescence Spectra and the Heterogeneous Emission of Alcohol Dehydrogenase†

Jay R. Knutson, Dana G. Walbridge, and Ludwig Brand*

ABSTRACT: A procedure is described for using nanosecond time resolved fluorescence decay data to obtain decay-associated fluorescence spectra. It is demonstrated that the individual fluorescence spectra of two or more components in a mixture can be extracted without prior knowledge of their spectral shapes or degree of overlap. The procedure is also of value for eliminating scattered light artifacts in the fluorescence spectra of turbid samples. The method was used to separate the overlapping emission spectra of the two tryptophan residues in horse liver alcohol dehydrogenase. Formation of a ternary complex between the enzyme, NAD^+, and pyrazole leads to a decrease in the total tryptophan fluorescence. It is shown that the emission of *both* tryptophan residues decreases. The buried tryptophan (residue 314) undergoes dynamic quenching with no change in the spectral distribution. Under the same conditions, the fluorescence intensity of tryptophan (residue 15) decreases without a change in decay time but with a red shift of the emission spectrum. There is also a decrease in tryptophan fluorescence intensity when the free enzyme is acid denatured (succinate buffer, pH 4.1). The denatured enzyme retains sufficient structure to provide different microenvironments for different tryptophan residues as reflected by biexponential decay and spectrally shifted emission spectra (revealed by decay association). The value of this technique for studies of microheterogeneity in biological macromolecules is discussed.

An important feature of the application of spectroscopic methods to biochemical problems is the ability to quantitatively assay and characterize individual components in a mixture. Identical chromophores often exhibit spectral differences due to environmental microheterogeneity. For example, proteins may exist in more than one conformational state, and this may be reflected in terms of different spectroscopic environments for tryptophan residues. Likewise, modifications of the physical state of a membrane may be revealed by altered spectroscopic characteristics of probe molecules.

Fluorescence spectroscopy has an advantage in this regard since both excitation and emission spectra are available. Matrix rank analysis of an array of emission spectra obtained at different exciting wavelengths has been used by Weber (1961) and Ainsworth (1961) to determine the number of emitting species in a mixture. Recently, Halvorson (1981) has described a significant factor analysis for such associations.

Fluorescence of organic molecules is characterized not only by unique excitation and emission spectra but also by signatory fluorescence decay times that may be dependent upon the microscopic environment. Advances in instrumentation and data analysis procedures have made it possible to obtain nanosecond time resolved emission spectra (TRES).[1] These represent fluorescence emission spectra obtained at specific times during the fluorescence decay. Ware et al. (1968, 1971) used either a stroboscopic photomultiplier or a gated single photon counting method to directly generate TRES by scanning emission spectra through a defined time window. Easter et al. (1976) have generated time-resolved emission spectra from decay curves obtained at 5-nm wavelength intervals. These decay curves were "deconvolved" by using the method of nonlinear least squares, and the TRES were reconstructed from the impulse response functions. This procedure is quite laborious but has the advantage of providing TRES free of convolution artifacts. Meech et al. (1981) have compared these two procedures for obtaining TRES and indicate the advantage of the former method for high energy resolution.

Nanosecond spectral shifts may have their origin in ground-state heterogeneity or microheterogeneity which may be revealed only in the emission of the excited state. In addition, spectral shifts may reflect excited-state reactions which take place on the nanosecond time scale. TRES have been used to study a variety of excited-state reactions (Ware et al., 1968; Easter et al., 1976; Gafni et al., 1976; Gafni & Brand, 1978; DeLuca et al., 1971; Laws & Brand, 1979).

It is important to distinguish two concepts—time-resolved emission spectra (TRES) and decay-associated spectra (DAS). The former are experimental emission spectra obtained during discrete time intervals following excitation. In contrast, DAS represent the spectral distributions of the individual emitting species which contribute to the total fluorescence. DAS are thus *derived* spectra uniquely linked to decay functions. DAS are the spectra the mixture would display if one could somehow exclude photons from all but one emitting species at a time.

If appropriate information is available regarding the nature of the complex decay behavior, the dimension of time can be utilized to qualitatively and quantitatively characterize biochemical mixtures which cannot be analyzed by spectral resolution alone. This is achieved by identifying decay functions uniquely associated with different species and then extracting spectra associated with those decays.

Phase-sensitive detection has been used by Lakowicz & Cherek (1981a) for resolution of heterogeneous fluorescence in binary systems. Eisinger (1969) utilized a similar technique on a quite different time scale to separate phosphorescence

† From the Department of Biology and McCollum-Pratt Institute, The Johns Hopkins University, Baltimore, Maryland 21218. *Received April 8, 1982.* This work was supported by National Institutes of Health Grant GM11632 and a fellowship to J.R.K. from the Pharmaceutical Manufacturers' Association Foundation. Publication No. 1155 from the McCollum-Pratt Institute. For a preliminary report of this work, see Knutson et al. (1981).

[1] Abbreviations: TRES, time-resolved emission spectra; DAS, decay-associated spectra; NAD^+, nicotinamide adenine dinucleotide; Trp, tryptophan; DPH, 1,6-diphenyl-1,3,5-hexatriene; ANTH, anthracene; 9-CNA, 9-cyanoanthracene; DML, dimyristoyl-L-α-phosphatidylcholine; NATA, *N*-acetyl-L-tryptophanamide; HLADH, horse liver alcohol dehydrogenase (EC 1.1.1.1); EDAS, excitation decay associated spectra; ADAS, anisotropy decay associated spectra.

0006-2960/82/0421-4671$01.25/0 © 1982 American Chemical Society

emissions from two different species. Lakowicz & Cherek (1981b) utilized their method to investigate the fluorescence of tryptophan and tyrosine derivatives and human serum albumin. They discuss the significance of this approach for studies of protein heterogeneity.

The aim of the present paper is to describe a rapid and simple pulse fluorometric method for obtaining high-resolution TRES. The theoretical foundation and data analysis procedure is described for obtaining *multiple* DAS (decay-associated spectra) from these data. The method is used to investigate the heterogeneous fluorescence of horse liver alcohol dehydrogenase.

Materials and Methods

Materials

Dimyristoyl-L-α-phosphatidylcholine (DML) vesicles, labeled with 1,6-diphenyl-1,3,5-hexatriene (DPH), were prepared in accordance with the procedure of Chen et al. (1977). Solutions of anthracene (ANTH) and 9-cyanoanthracene (9-CNA) were prepared, both separately and mixed, as ethanol (Pharmco) solutions. Anthracene was obtained from Aldrich and recrystallized twice from ethanol. 9-CNA was obtained from Aldrich and used without further purification. Both fluorophores were examined for fluorescent purity, and each compound exhibited a single exponential decay component whose lifetime was the same whether mixed or alone. The final concentrations studied were 2×10^{-6} M 9-CNA and 1.3×10^{-5} M ANTH. The absorbances of these solutions were below 0.1 in both excitation and emission regions. Horse liver alcohol dehydrogenase (HLADH) was obtained from Boehringer Mannheim and was prepared as described previously (Ross et al., 1981). *N*-Acetyl-L-tryptophanamide (NATA) was purchased from Vega Biochemicals and used as a fluorescent standard during the HLADH measurements (1×10^{-4} M NATA in 0.05 M sodium phosphate buffer, pH 7.4).

Methods

The single photon counting pulse fluorometer has been described elsewhere (Badea & Brand, 1979). It accumulates a decay histogram of photon counts (intensity) vs. time of photon arrival. The time axis, whose zero is electronically set to precede the excitation flash, is split into small (typically 0.1–0.2 ns) "channels". Thus, one can establish a "time window" by summing the photon counts over any desired group of channels in the decay curve. Alternatively, one may connect a parallel circuit which accepts only photons within a preset window. While the latter method (single channel analyzer) is simple to implement and served as a prototype for developing the method, it is only a "time censor" which discards photons at all other times. In the "channel-summing" window method, all time-dependent information is collected simultaneously. Then, under software control,[2] the channels are sorted into windows for totalizing. Thus, economy of collection time is gained along with the assurance that time-windowed spectra were collected under identical instrument and sample conditions. Spectra are generated by stepping the emission monochromator to the next wavelength after each brief accumulation of photons into the time windows. When the entire wavelength range has been spanned, *all* of the time-windowed spectra will have been accumulated. For example, windowed spectrum "A" will be kept in computer memory as the sum of counts in channel "group A" vs. wavelength step.

The separation of a heterogeneous fluorescence decay (at a single wavelength) into its underlying decay components has been discussed elsewhere (Badea & Brand, 1979). While many numerical methods can be used to provide estimates for experimental decay rates, we have found that the method of nonlinear least squares is both adaptable and demonstrably reliable. As will be discussed under Theory, the shape of the decay function for an *individual* species in a heterogeneous system is wavelength independent. Decay-associated spectra are, therefore, dependent on our ability to measure the overall decay response and deduce the underlying decay functions for association.

All measurements on the single photon counting pulse fluorometer were obtained under "magic angle" polarization conditions (Badea & Brand, 1979) to exclude errors from Brownian rotation. Fluorescence decay time measurements of NATA and HLADH were obtained contemporaneously, under identical optical and instrumental conditions. The wavelength-dependent time shifts between excitation and emission wavelengths were determined through multiple (variation of the time shift parameter) analyses of the NATA standard.

Theory

Theory of Spectral Separation. Fluorescence emission intensity is a function of both wavelength (inverse of energy) and time after excitation. For a *homogeneous* emitting population, this total intensity can be separated into the product of a wavelength distribution with a time distribution:

$$f(\lambda,t) = \alpha(\lambda)d(t) \tag{1}$$

(Separation of variables is justified only for *homogeneous* components. In heterogeneous systems, spectral shapes may be time dependent, or decay shapes may be wavelength dependent.) In many important systems, the decay coefficient is a constant whose inverse is the lifetime (τ) of the excited state:

$$f(\lambda,t) = \alpha(\lambda)e^{-t/\tau} \tag{1a}$$

The case of exponential decay is most frequent, so we will focus on $d(t) = e^{-t/\tau}$.

Separation of decay-associated spectra, however, does *not* depend on the functional shape of $d(t)$, and we will also show how multiexponential and nonexponential cases can be studied.

A single binary mixture of fluorophores leads to a time-varying spectrum and a wavelength-dependent decay:

$$f(\lambda,t) = \alpha_1(\lambda)e^{-t/\tau_1} + \alpha_2(\lambda)e^{-t/\tau_2} = \sum_{i=1}^{2}\alpha_i(\lambda)e^{-t/\tau_i} \tag{2}$$

The theoretical decay functions discussed are *impulse* responses, i.e., the decay of intensity that follows instantaneous excitation. Most light sources used for pulse fluorometry, however, have significant effective width on the nanosecond time scale. Thus, the decay of intensity following experimental excitation events is more complex. Qualitatively, the lamp flash can be divided into a sequence of "instantaneous" flashes, each of which generates a decay response. The sum of all of these responses is the *observed* decay function D. In the limit of continuous subdivision, D is the *convolution* ("faltung") of the impulse function d with the lamp $L(t)$:

$$D(t') = \int_0^{t'} L(t)d(t' - t)\,dt \tag{3}$$

Thus, in the single exponential case

$$F_{obsd}(\lambda,t') = \alpha(\lambda)\int_0^{t'} L(t)e^{-(t'-t)/\tau}\,dt = \alpha(\lambda)D(t') \tag{4}$$

[2] The computer programs used for data collection and data analysis are written in Fortran IV for use with an HP System 1000 (21MX) computer. The software will be made available upon request to the authors.

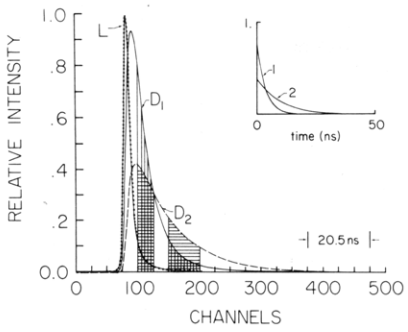

FIGURE 1: Procedure for determination of mixing coefficients used to extract DAS from TRES. L is the lamp profile, D_1 is the convolved decay due to component 1, D_2 is the convolved decay due to component 2, and curves 1 and 2 in the inset are the corresponding impulse response functions. The shaded areas define mixing coefficients, as indicated in eq 6. Each channel spans 0.205 ns. D_1 = anthracene, D_2 = 9-cyanoanthracene. Excitation was at 357 nm and emission at 420 nm. The temperature was 25 °C, and the solvent was ethanol.

Notice that the spectral features are unaffected by convolution; i.e., convolution acts on the (wavelength-independent) decay function *only*. For the heterogeneous case, we observe

$$F(\lambda,t') = \sum_i \left[\alpha_i(\lambda) \int_0^{t'} L(t) e^{-(t'-t)/\tau_i} \, dt \right] = \sum_i [\alpha_i(\lambda) D_i(t')] \tag{5}$$

At any time t' on the instrumental observation scale, the emission is a mixture of the constituent spectra $\alpha_i(\lambda)$, with mixing coefficients $D_i(t')$. In practical cases, we actually observe a time "slice" (e.g., from $t' = a$ to $t' = b$). In this case, the correct mixing coefficients C_i are integrals from a to b of the observed decay components D_i:

$$C_i(a \rightarrow b) = \int_a^b D_i(t') \, dt' = \int_{t'=a}^{t'=b} \left[\int_0^{t'} L(t) e^{-(t'-t)/\tau_i} \, dt \right] dt' \tag{6}$$

and the mixed spectrum seen in this time slice is

$$F(\lambda,a \rightarrow b) = \sum_i \alpha_i(\lambda) C_i(a \rightarrow b) \tag{7}$$

$F(\lambda,a \rightarrow b)$ is the spectrum obtained by summing all photons between instrument time channels a and b, and $C_i(a \rightarrow b)$ is the time-dependent mixing coefficient for component $\alpha_i(\lambda)$.

Time-resolved emission spectra obtained over two different time windows, $a \rightarrow b$ and $c \rightarrow d$, provide sufficient information to resolve two decay-associated spectra.

According to eq 5, we may write expressions for the TRES obtained in slices $a \rightarrow b$ and $c \rightarrow d$:

$$F(\lambda,a \rightarrow b) = \alpha_1(\lambda) C_1(a \rightarrow b) + \alpha_2(\lambda) C_2(a \rightarrow b) \tag{8}$$

$$F(\lambda,c \rightarrow d) = \alpha_1(\lambda) C_1(c \rightarrow d) + \alpha_2(\lambda) C_2(c \rightarrow d) \tag{9}$$

Equation 8 defines the TRES obtained in the interval $a \rightarrow b$, and eq 9 defines the TRES obtained from $c \rightarrow d$. Clearly, these TRES contain contributions due to each emitting species but in different proportions. The mixing coefficients C_1 and C_2 are defined in eq 6. They can be calculated from a fluorescence decay analysis at any particular wavelength. In the exponential case, the decay analysis provides α_1, τ_1, and α_2, τ_2 at that wavelength.

As indicated in Figure 1, the impulse response, $f_1 = \alpha_1 e^{-t/\tau_1}$, is convolved with the lamp flash $L(t)$, giving curve D_1. A similar operation gives curve D_2 from α_2 and τ_2.

The mixing coefficients $C_1(a \rightarrow b)$ and $C_2(a \rightarrow b)$ are the areas under curves D_1 and D_2 over the time intervals $a \rightarrow b$. The coefficients $C_1(c \rightarrow d)$ and $C_2(c \rightarrow d)$ are obtained in a corresponding manner. Since the TRES $F(\lambda,a \rightarrow b)$ are obtained in convolved space, it is also necessary to obtain the mixing coefficients in convolved space.

Equations 8 and 9 provide two equations which can be solved for the two unknown decay-associated spectra:

$$\alpha_1(\lambda) = [[C_2(c \rightarrow d)/C_2(a \rightarrow b)] F(\lambda,a \rightarrow b) - F(\lambda,c \rightarrow d)]/K_1 \tag{10}$$

$$\alpha_2(\lambda) = [[C_1(c \rightarrow d)/C_1(a \rightarrow b)] F(\lambda,a \rightarrow b) - F(\lambda,c \rightarrow d)]/K_2 \tag{11}$$

where

$$K_1 = [C_2(c \rightarrow d)/C_2(a \rightarrow b)] C_1(a \rightarrow b) - C_1(c \rightarrow d) \tag{10a}$$

and

$$K_2 = [C_1(c \rightarrow d)/C_1(a \rightarrow b)] C_2(a \rightarrow b) - C_2(c \rightarrow d) \tag{11a}$$

Once the decay-associated spectra $\alpha_i(\lambda)$ have been obtained, one can always reconstruct deconvolved TRES at any time after (impulse) excitation $\tilde{t}$:

$$f(\lambda,\tilde{t}) = \alpha_1(\lambda) e^{-\tilde{t}/\tau_1} + \alpha_2(\lambda) e^{-\tilde{t}/\tau_2} = \sum_i \alpha_i(\lambda) d_i(\tilde{t}) \tag{12}$$

Once we know the underlying DAS, reconstruction of impulse TRES is only a matter of properly mixing DAS contributions, where $\tilde{t}$ is the time at which the TRES are described. If one wishes TRES to span an impulse time window $\tilde{t}_a \rightarrow \tilde{t}_b$, replace $e^{-\tilde{t}/\tau_i}$ with $\int_{\tilde{t}_a}^{\tilde{t}_b} e^{-t/\tau_i} \, dt$ in eq 12.

Three or More Components. If the aggregate spectrum is composed of three spectra [$\alpha_1(\lambda)$, $\alpha_2(\lambda)$, and $\alpha_3(\lambda)$], they can be derived from the information contained in three TRES:

$$F(\lambda,a \rightarrow b) = \alpha_1(\lambda) C_1(a \rightarrow b) + \alpha_2(\lambda) C_2(a \rightarrow b) + \alpha_3(\lambda) C_3(a \rightarrow b) \tag{13a}$$

$$F(\lambda,c \rightarrow d) = \alpha_1(\lambda) C_1(c \rightarrow d) + \alpha_2(\lambda) C_2(c \rightarrow d) + \alpha_3(\lambda) C_3(c \rightarrow d) \tag{13b}$$

$$F(\lambda,e \rightarrow f) = \alpha_1(\lambda) C_1(e \rightarrow f) + \alpha_2(\lambda) C_2(e \rightarrow f) + \alpha_3(\lambda) C_3(e \rightarrow f) \tag{13c}$$

or

$$F(\lambda,j) = F_j(\lambda) = \sum_{i=1}^{3} C_{ji} \alpha_i(\lambda) \tag{13d}$$

where we have replaced the window specifications with an index j. The solution of eq 13a–c is obtained by inverting the matrix of area coefficients C_{ji}. Then

$$\alpha_m(\lambda) = \sum_{k=1}^{3} G_{mk} F_k(\lambda) \tag{14a}$$

where G_{mk} is the matrix inverse of C_{ji}. This inversion can be carried out in many ways. DAS are thus the solution of n equations in n unknowns, where n is the number of underlying components. The constants for these equations are obtained from the decay functions as described in eq 4–6.

We would also like to suggest that the matrix inversion approach used to compute DAS should also prove useful in the analysis of phase-sensitive spectra. In this case, the coefficients C_{ji} in eq 13d will be replaced by

$$C(\omega)_{ji} = K_i(\omega) \cos(\phi_i - \phi_j) \tag{14b}$$

where K_i is the species-specific (constant) modulation factor and ϕ_i the phase of the ith constituent, while ϕ_j is the phase angle of observation. The binary spectral separations effected by phase-sensitive detection in the past have been based on setting $\phi_i - \phi_j = \pm 90°$, eliminating one of *two* components. The more general matrix inversion approach outlined above will not be restricted to binary systems. Knowledge of the component phases (ϕ_i) depends, however, on an accurate heterogeneity analysis of the total fluorescence, and current

phase fluorometers have not been used for ternary decay analysis. Careful multiwavelength overdetermination of system transfer function parameters should, however, yield this information.

Special Cases: Scattered Light and Excited-State Reaction. In the case of scattered light, $d_s(t)$ must be an instantaneous response. In this situation, the scattered excitation profile is a constant multiple of the lamp profile:

$$f_s(\lambda,t) = \alpha_s(\lambda)d_s(t) = \alpha_s(\lambda)\delta(t) \quad (15)$$

$$D_s(t') = \int_0^{t'} L(t)\delta(t'-t)\,dt = L(t') \quad (16)$$

$$C_s(x\rightarrow y) = \int_x^y L(t')\,dt' \quad (17)$$

In the well-known [for a review, see Badea & Brand (1979)] two-state excited-state reaction, *both* emitting species have biexponential kinetics, and they share the same exponential decay rates:

$$A(\lambda,t) = \alpha_A(\lambda)d_A(t) = [\eta_1 e^{-t/\tau_1} + \eta_2 e^{-t/\tau_2}]\alpha_A(\lambda) \quad (18)$$

$$B(\lambda,t) = \alpha_B(\lambda)d_B(t) = [\beta e^{-t/\tau_1} - \beta e^{-t/\tau_2}]\alpha_B(\lambda) \quad (19)$$

η_1, η_2, β, τ_1, and τ_2 are as explained in Laws & Brand (1979).

In this case, we need to use more than the α_i, τ_i recovered from decay measurement; in fact, the DAS one extracts for τ_1 and τ_2 are each simple combinations of $\alpha_A(\lambda)$ and $\alpha_B(\lambda)$:

$$\alpha_1(\lambda) = \eta_1\alpha_A(\lambda) + \beta\alpha_B(\lambda) \quad (20)$$

$$\alpha_2(\lambda) = \eta_2\alpha_A(\lambda) - \beta\alpha_B(\lambda) \quad (21)$$

Notice, however, that the B species contributions to DAS α_1 and DAS α_2 are *equal* and *opposite*. Thus, for this pure two-state interchange (where B is not excited directly), one can directly calculate the A spectrum:

$$\alpha_A(\lambda) = [\alpha_1(\lambda) + \alpha_2(\lambda)]/(\eta_1 + \eta_2) \quad (22)$$

Similarly

$$\alpha_B(\lambda) = [\eta_2\alpha_1(\lambda) - \eta_1\alpha_2(\lambda)]/[(\eta_2 + \eta_1)\beta] \quad (23)$$

Notice that we can deduce the shape of $\alpha_A(\lambda)$ directly, while $\alpha_B(\lambda)$ can be solved for when the ratio η_1/η_2 is known. The knowledge of α_A, however, permits one to solve for α_B by difference, and η_1/η_2 can often be measured directly at the blue edge. In particular, for the simple irreversible case, $\eta_1 = 0$.

For certain cases (such as proton transfer), the ratio η_1/η_2 can also be obtained with one separate decay measurement:

$$\eta_1/\eta_2 = [1/\tau_2 - (k_A + k)]/[(k_A + k) - 1/\tau_1] \quad (24)$$

where $k_A + k$ can be obtained from the plot $1/\tau_1 + 1/\tau_2$ vs. $1/(\tau_1\tau_2)$ (Badea & Brand, 1979).

As an alternative to the above approach, one could use separate knowledge of amplitude ratios along with eq 18 and 19 to construct $d_A(t)$ and $d_B(t)$ decay functions. Then one could use eq 3 to calculate convolved space decays $D_A(t')$ and $D_B(t')$, which could be integrated in eq 6 to calculate C_A and C_B factors for windowed TRES. Then, in the same way as for the simple exponential case, one could solve *directly* for $\alpha_A(\lambda)$ and $\alpha_B(\lambda)$ (see eq 10–12).

The latter method is the method of choice when one cannot be assured that eq 20 and 21 hold; for example, if some of the excited species B is formed by direct excitation, $d_B(0) \neq 0$. Conversely, the former method can serve as a test for $d_B(0)$. The latter method is also applicable to the *general* set of $d_i(t)$ functions (multiple exponential or even *non*exponential decays). The most stringent requirement is that one must identify the $d_i(t)$ functions that characterize the individual emitting species.

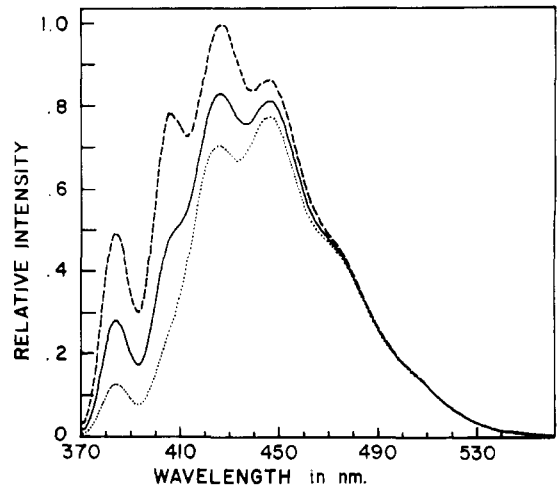

FIGURE 2: Steady-state and nanosecond time resolved emission spectra (TRES) obtained with a mixture of anthracene (1.3×10^{-5} M) and 9-cyanoanthracene (2×10^{-6} M) in ethanol at 25 °C. The solid curve is the steady-state spectrum. The dashed curve is an "early" time-windowed spectrum, taken between channels 1 and 122 (see Figure 1), and the dotted curve is a "late" time-windowed spectrum, taken between channels 123 and 510. The spectra were normalized at 500 nm.

Results

In order to test the veracity of the spectra derived as described above, we chose to examine the mixed emission of anthracene and 9-CNA, two fluorophores with a moderate difference in decay times (4.1 and 11.7 ns, respectively). Anthracene shows structured emissions in a region where 9-cyanoanthracene does not emit. Thus, even small spectral contamination in the generated DAS should be clearly evident. Figure 2 shows the time-resolved emission spectra obtained with this mixture over early and late time windows. The steady-state spectrum of the mixture is included for comparison. The emission of anthracene predominates at early times, while the emission due to anthracene makes a smaller contribution (compared to 9-cyanoanthracene) at a late time window. The decay-associated spectra (DAS) generated from the time-resolved data (TRES) by the procedures described above are shown in Figure 3. The normalized fluorescence spectra obtained with individual solutions of anthracene and 9-cyanoanthracene are shown as solid lines and may be compared with the DAS obtained from the mixture, shown as open and closed circles. Any remaining spectral contamination of the 9-cyanoanthracene emission by anthracene would be clearly evident if present.

The decay-association approach described here can also be used to remove the artifactual contributions to emission spectra made by scattered excitation light in turbid solutions. As an example, Figure 4 shows the steady-state fluorescence emission spectrum of DPH in a turbid suspension of dimyristoyllecithin (DML) vesicles. The spectrum decay associated with the decay of DPH shows no contributions due to scattered light. This spectrum is superimposable with the normalized spectrum obtained by excitation at a more remote wavelength. This altered excitation approach is possible in this pure lipid system but may not be available in a real biological membrane, due to autofluorescence.

Decay-associated emission spectroscopy should be of particular value for studies of microheterogeneity of protein fluorescence. In this case, the spectra of the individual components are not independently available. As an example, Figure 5 (left panel) shows the steady-state fluorescence emission spectrum of horse liver alcohol dehydrogenase

Table I: Integrated Areas under the Total Emission and DAS for HLADH under Various Conditions[a]

condition	areas under spectra, in arbitrary units			decay times (ns)	
	total	component 1	component 2	τ_1	τ_2
native[b]	49.2 (100)	27.4 (100)	21.8 (100)	3.8 (100)	6.7 (100)
+NAD^+, pyrazole[b]	30.4 (62)	18.5 (68)	11.9 (55)	2.4 (63)	7.0 (104)
denatured[c]	20.8 (42)	7.7	13.2	2.0	5.3

[a] The values in parentheses are percentages and refer to the percent remaining. [b] Average of three experiments. [c] Average of two experiments.

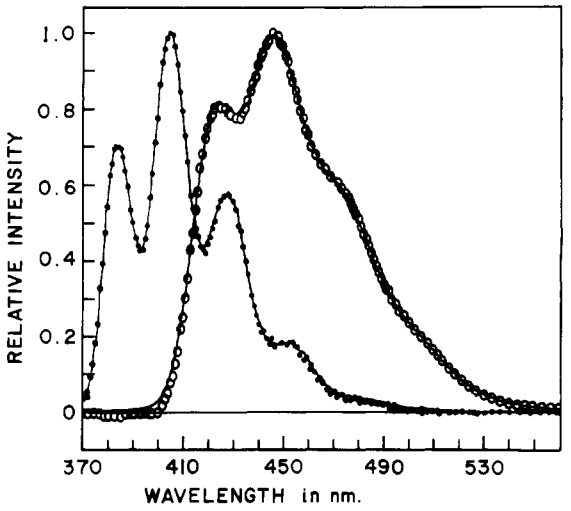

FIGURE 3: Decay-associated fluorescence emission spectra (DAS) obtained from the TRES shown in Figure 2. The solid curves are the fluorescence spectra obtained in separate experiments with solutions of pure anthracene and pure 9-cyanoanthracene. The solid circles represent the normalized DAS for component 1 (anthracene), and the open circles are the normalized DAS for component 2 (9-cyanoanthracene).

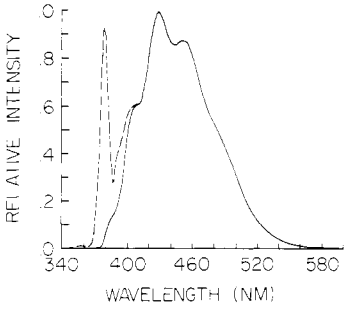

FIGURE 4: DAS methodology used to remove a scatter contribution from the emission spectrum of a turbid sample. The sample contained single bilayer vesicles made from DML (1.5 mM in lipid) labeled with DPH (3×10^{-6} M) in 0.01 M Tris-HCl and 0.1 M NaCl, pH 7.4. Excitation was at 380 nm. The dashed curve shows the distorted steady-state spectrum, and the solid curve is the DAS for the fluorescent component (DPH).

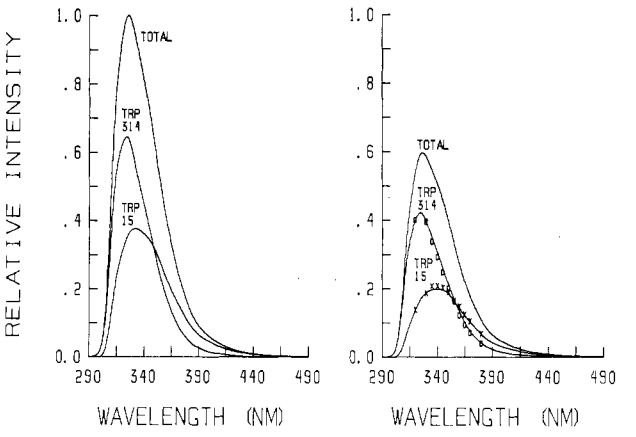

FIGURE 5: (Left panel) Steady-state (total) and decay-associated emission spectra for horse liver alcohol dehydrogenase. The cuvettes contained $\sim 1 \times 10^{-5}$ M HLADH ($\epsilon_{280} = 3.53 \times 10^4$) in 0.05 M sodium phosphate, pH 7.4 at 10 °C. Excitation was at 295 nm. (Right panel) Steady-state and decay-associated emission spectra of native HLADH ($\sim 1 \times 10^{-5}$ M in 0.05 M sodium phosphate, pH 7.4) in the presence of NAD^+ ($\sim 2 \times 10^{-5}$ M) and pyrazole ($\sim 2 \times 10^{-4}$ M) at 10 °C. Correction was made for the slight dilution caused by adding NAD^+ and pyrazole to the sample. For comparison, (×) and (○) are the two component amplitudes derived from the individual (complete) decay curves taken at the wavelengths indicated, using $\alpha_i\tau_i/(\alpha_1\tau_1 + \alpha_2\tau_2)$ to subdivide the steady-state intensity. The DAS were numerically smoothed to remove high-frequency noise and normalized to $\alpha_i\tau_i$ at 350 nm.

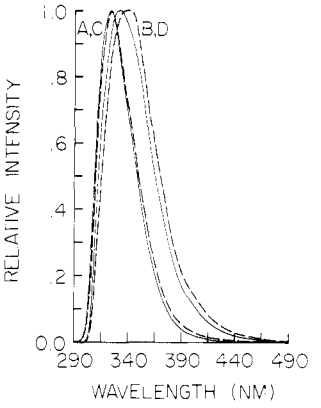

FIGURE 6: Peak-normalized decay-associated emission spectra for HLADH in the absence (A and B, solid lines) and presence (C and D, dashed lines) of NAD^+ and pyrazole, showing the altered spectrum of Trp-15. Conditions were identical with those indicated for Figure 5.

(HLADH) together with the decay-associated emission spectra corresponding to emission from the buried (Trp-314) and exposed (Trp-15) tryptophan residues. It was previously reported (Ross et al., 1981) that HLADH shows double-exponential decay and that each decay time could be associated with a specific tryptophan residue. The data shown in Figure 5 (right panel) indicate a decrease in the fluorescence intensity upon ternary complex formation with NAD^+ and pyrazole. The fluorescence intensity of *both* the buried and the exposed tryptophan decreases. This is of interest in view of the fact that (as indicated in Table I) only the decay time associated with the buried tryptophan decreases on ternary complex formation. The small increase in decay times found for the exposed tryptophan before and after ternary complex formation may not be distinguished from analysis error since, with the native enzyme, τ_1 and τ_2 are rather close. The results for repeat experiments shown in Table II confirm the slightly larger lifetime uncertainty associated with native as compared to complexed enzyme. The peak-normalized DAS for native enzyme and for the ternary complex (Figure 6) show that the dynamic quenching of Trp-314 is not associated with a significant spectral shift, while the decrease in fluorescence intensity of Trp-15 is associated with a definite red shift.

Table II: Emission Decay Parameters and Their Standard Deviations for HLADH under Various Conditions[a]

sample	expt no.	χ^2	α_1	τ_1	α_2	τ_2	α(scatter)
native HLADH	1	1.48	0.609 ± 0.037	3.70 ± 0.11	0.391 ± 0.040	6.58 ± 0.15	0.009
	2	1.63	0.659 ± 0.033	3.96 ± 0.09	0.341 ± 0.037	6.86 ± 0.15	0.012
	3	1.66	0.622 ± 0.028	3.75 ± 0.09	0.378 ± 0.016	6.73 ± 0.12	0.004
			<0.630>[b]	<3.80>	<0.370>	<6.72>	<0.008>
HLADH + NAD$^+$, pyrazole	1	1.23	0.759 ± 0.006	2.38 ± 0.03	0.241 ± 0.007	6.85 ± 0.07	0.021
	2	1.13	0.786 ± 0.005	2.44 ± 0.03	0.214 ± 0.006	7.08 ± 0.06	0.003
	3	1.43	0.774 ± 0.004	2.39 ± 0.02	0.226 ± 0.005	7.09 ± 0.05	0.022
			<0.773>	<2.40>	<0.227>	<7.01>	<0.015>
acid-denatured HLADH	1	1.54	0.584 ± 0.007	1.92 ± 0.04	0.416 ± 0.009	5.31 ± 0.04	0.045
	2	1.43	0.574 ± 0.008	1.99 ± 0.05	0.426 ± 0.011	5.30 ± 0.04	0.056
			<0.579>	<1.96>	<0.421>	<5.31>	<0.051>

[a] HLADH was in 0.05 M sodium phosphate, pH 7.4. For the ternary complexes, [NAD$^+$] was 2 times the site concentration and [pyrazole] 10 times the site concentration. The denatured HLADH was in 0.1 M sodium succinate buffer at pH 4.1. The HLADH concentration varied between experiments, from 0.8×10^{-5} to 1.4×10^{-5} M. Excitation was at 295 nm, emission was at 350 nm, and the temperature was 10 °C. The emission half-bandwidth was 10 nm. The decay curves were collected to (10–15) $\times 10^3$ counts at the peak. The values listed for χ^2 are the goodness to fit statistics as described by Bevington (1969), and the monovariate standard deviation *estimates* (which differ from precision) are described on p 154 of the same book. [b] Values in broken brackets are averages.

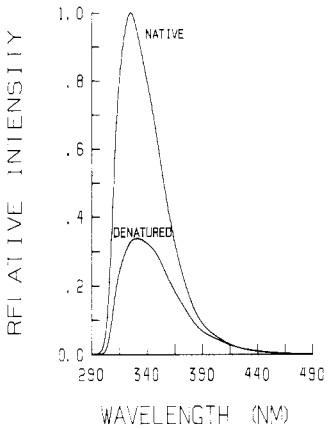

FIGURE 7: Steady-state fluorescence emission spectra of native HLADH and the enzyme denatured in 0.1 M sodium succinate buffer at pH 4.1. (The enzyme was allowed to denature for 1 h at 10 °C. The spectra were taken at 10 °C. Both samples are $\sim 1 \times 10^{-5}$ M in HLADH and are corrected for dilution differences.)

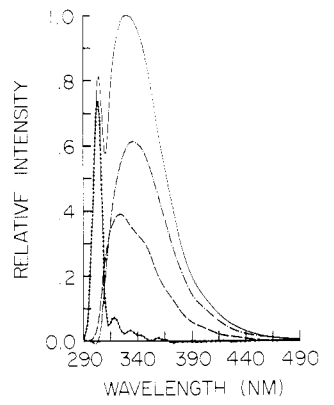

FIGURE 8: Decay-associated spectra derived from a three-component analysis (two fluorescent, one scatter) of denatured HLADH ($\sim 1 \times 10^{-5}$ M). The dotted curve represents the contribution associated with scattered exciting light.

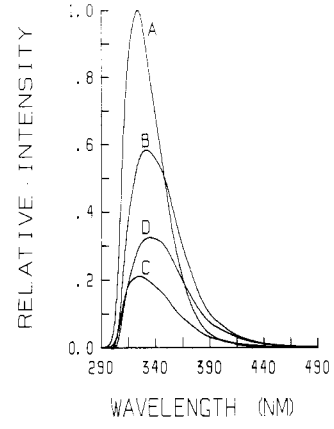

FIGURE 9: Decay-associated fluorescence spectra for native (A and B) and denatured (C and D) HLADH. Conditions are as indicated for Figure 7. For ease of visualization, only fluorescent components are shown.

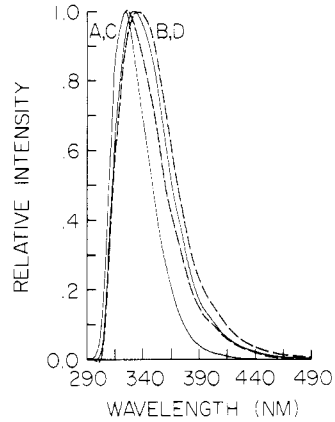

FIGURE 10: Peak-normalized decay-associated spectra for native and denatured HLADH of Figure 9.

It is known that HLADH undergoes a time-dependent (minute time scale) denaturation in succinate buffer at pH 4 (Heitz & Brand, 1971). Figure 7 shows the significant decrease in tryptophan fluorescence intensity which accompanies this denaturation. It was of interest to ask if the denatured enzyme still retains sufficient structure to place tryptophan residues in more than one microenvironment. The results shown in Figures 8 and 9 indicate that it is possible to decay associate the fluorescence of the denatured protein into two bands. The normalized DAS given in Figure 10 show that *both* decay-associated spectra are different from the DAS observed with the native enzyme. The acid-denatured HLADH showed some turbidity. As is shown in Figure 8, this adds a significant scatter contribution to the steady-state emission spectrum (solid line). For this reason, we used a *three*-component analysis to derive the DAS (as described under Theory). Spectra associated with the two decay times (dashed lines) and the spectrum associated with the lamp profile (dotted line) are shown. For convenience of presen-

tation, the scattered light components are not included in Figures 9 and 10.

Discussion

Spectroscopic methods such as fluorescence are useful tools for studies of heterogeneity of proteins and membranes. Fluorescence emission spectra often reflect the degree to which chromophores are exposed to solvent. Even fluorophores that are shielded from solvent can exhibit spectral shifts due to specific environmental interactions.

The theory and instrumental methods described here provide a pulse fluorometric technique for associating unique fluorescence emission spectra with specific fluorescence decay times *observed* in a mixture of emitting species. It should be emphasized that this is achieved *without* prior knowledge of the shape of the emission spectra of the individual species. It is of interest to determine whether observed multiexponential decay kinetics have their origin in ground-state heterogeneity or in an excited-state reaction. As was indicated above, decay-associated spectra may also aid in distinguishing between these two cases.

The experimental data required to generate n decay-associated spectra (DAS) are n time-resolved emission spectra (TRES) and a decay measurement at some wavelength capable of resolving the n decay functions. (In practice, it is wise to examine decays at a few more wavelengths.) The ability to resolve spectra is directly related to the ability to resolve decay times. This will depend both on the number of decay parameters and on their degree of correlation. In general, if decay times differ by a factor of 2 or more, they are readily separable by most methods of analysis (Gafni et al., 1975) for even a *single* decay curve. Decay times closer in size can be resolved by analyzing *multiple* decay curves at several wavelengths with the restriction that the decay times do not change with wavelength while the amplitudes do vary.

The various emission spectra in a mixture can be resolved if one can obtain n emission spectra containing different fractional contributions from each component. This is the information provided by the n TRES. Since each component to be spectrally resolved must have a different decay, each TRES will then provide an emission spectrum containing a *different* mixture of the components. TRES obtained by the pulse method are usually produced by a lamp flash of finite width, so the "true" impulse time window is ill-defined. For this reason, each individual lifetime is extracted from a total decay experiment. Then each term is individually convolved with the lamp profile (as shown in Figure 1), and this *convolved* information is used to calculate the mixing coefficients described earlier. It should be reiterated at this point that TRES are experimentally determined, mixed emission spectra. In contrast, DAS are derived ("unmixed") spectra and exploit knowledge of the underlying decay functions in the mixture. In the examples described in this report, independent information allowed for the assignment of two measured decay times to two ground-state species. While no examples of the application to excited-state heterogeneity are presented in this paper, it is apparent (see Theory) that DAS will reveal those features as well.

Alcohol dehydrogenase from horse liver is a well-studied enzyme. The X-ray structure has been determined (Brändén et al., 1975), and considerable information is available about its solution biochemistry. The protein is a dimer made up of identical subunits. Each monomer contains two tryptophan residues. One of the tryptophans is well exposed to solvent (Trp-15) while the other (Trp-314) is buried in a cage of hydrophobic residues at the dimer interface between the subunits (Abdallah et al., 1978). Double-exponential fluorescence decay kinetics are observed with the native enzyme, and a long decay (near 7 ns) has been assigned to Trp-15 while the short decay (near 3.8 ns) has been assigned to the buried residue (Trp-314) (Ross et al., 1981). The procedure described here has been used to rapidly generate the decay-associated emission spectra (DAS) for each of these tryptophan residues, giving the same result as that reported previously with the use of a more laborious method that required obtaining many complete decay curves across the entire emission spectrum (Ross et al., 1981). A smaller set of such measurements is included for comparison in Figure 5. These DAS show that with excitation at 295 nm, the exposed tryptophan shows lower fluorescence intensity than the buried residue, Trp-314. While "solvent relaxation" cannot be excluded as a source of much smaller nanosecond shifts for each residue, it is clear that simple heterogeneity predominates.

Formation of the ternary complex between HLADH, NAD^+, and pyrazole decreases the tryptophan fluorescence intensity. Only the short decay time, attributed to the buried Trp-314, is decreased. The DAS shown in Figure 5 indicate that the *intensity* of emission of *both* tryptophans is decreased. The normalized DAS shown in Figure 5 show that Trp-314 retains its spectral shape, while Trp-15 exhibits a spectral red shift in the complex. The decrease in fluorescence of Trp-15 without a concomitant decrease in the decay time of this residue may be attributed to either static quenching or to a decrease in the absorbance of Trp-15 at 295 nm.

The fact that the shape of the emission spectrum of Trp-314 remains essentially unchanged upon ternary complex formation with NAD^+ and pyrazole is consistent with the proposal by Ross et al. (1981) that resonance energy transfer might have a key role in the dynamic quenching of this residue. It is of interest that the microenvironment of Trp-15 in the ternary complex is such that the remaining emission is shifted to the red compared to Trp-15 in the native enzyme. This shift may be related to the finding of Eklund et al. (1976) that Trp-15 becomes more exposed to solvent upon ternary complex formation. Eftink & Selvidge (1982) report a reduction in the ability of acrylamide to quench Trp-15 upon formation of the ternary complex (with trifluoroethanol). They suggest that this change may arise in part from the direct quenching of the residue in the complex. This is in accord with our finding of reduced Trp-15 fluorescence in the ternary (pyrazole) complex. Laws & Shore (1978) have also examined the ternary complex with trifluoroethanol, using iodide as a quencher.

Vallee & Hoch (1957) showed that HLADH loses Zn atoms at pH below 6 and undergoes denaturation. Blomquist (1967) and Heitz & Brand (1971) showed that the denaturation caused a decrease in tryptophan fluorescence intensity and that this could be used to investigate the kinetics of acid denaturation. The denatured enzyme still appears to exhibit biexponential decay kinetics, and the DAS are shown in Figures 9 and 10 together with the DAS obtained with the native enzyme. It is of interest that the denatured molecule retains sufficient structure to place tryptophan residues in different microenvironments, as reflected by different decay times and different decay-associated emission spectra. In this case, we have not yet assigned the observed ground-state heterogeneity to specific tryptophan residues.

Fluorescence emission is characterized in terms of excitation and emission spectra as well as decay times and emission anisotropy. Each of these parameters is subject to perturbation by the microenvironment. This provides a powerful tool for revealing microheterogeneity. Although any individual pa-

rameter may not be capable of resolving different species, the *combination* of parameters provided by association may be used to achieve this end. For example, the linkage between excitation and emission spectra as determined by matrix rank methods (Weber, 1961; Ainsworth, 1961) has been used to evaluate the number of fluorescent components in a mixture. The present paper describes a simple instrumental method and procedures for data analysis that can be used to obtain decay-associated fluorescence *emission* spectra. The identical framework described here can be used to derive decay-associated excitation spectra (EDAS) or anisotropy decay associated spectra (ADAS for either excitation or emission). An advantage of DAS and EDAS is that heterogeneity in *either* emission *or* absorption spectra alone can be detected, whereas matrix rank analyses require significant heterogeneity in both spectra. We have exploited ADAS to investigate the rotational heterogeneity of DPH binding to different lipid domains (Knutson et al., 1982a).

In view of the multiple associations that can be established, it is interesting to consider the various features of associated spectra that can add extra insight into the *mechanism* of heterogeneity. For example, a binary heterogeneous decay can arise either from different ground-state species or from duality that is generated in the excited state. The latter case is manifested by a species whose excited-state concentration rises and then falls, leading to a negative preexponential (see eq 19). This negative term can be masked in the overlap region between the two excited-state spectra, and the overlap may persist until both spectra are greatly diminished. However, as eq 21 shows, the DAS for component 2 will be *negative* where the B state dominates. There is another special hallmark of the excited-state reaction case: if only one ground-state species is excited, then the decay-associated excitation spectra must be identical for all emission wavelengths. Decay-associated spectra are therefore able to reveal sources as well as the degree of heterogeneity.

DAS, or any other form of associated information, are derived quantities. Thus, it is important to be certain of the decay functions that are used. Decay functions that are in error quite naturally yield incorrect spectra. These errors, however, are easily monitored and eliminated. The accuracy of the underlying functions can and should be verified by decay analysis at more than one wavelength (changing wavelength to overdetermine time parameters). Alternatively, one can use, as we have, *more* than n TRES to resolve n DAS. In the latter case, agreement between DAS from several different window locations is strong evidence that the decay functions and DAS are both correct (changing time windows to overdetermine spectra). We have found that both overdetermination techniques are helpful. Thus, confidence in DAS requires only customary levels of precaution. In the case of continuous dipolar relaxation (DeToma et al., 1976), it is not clear that unique decay functions can be selected for DAS. Inappropriate associations will lead to a dependence of results on window choice, and these inconsistent spectra can be used to reject the attempted association. Thus, continuous relaxation is a complicating but identifiable problem. When discovered, it demands a more detailed time-resolution study than do heterogeneous systems.

The information required to understand the fluorescence of a biochemical system is contained in a high-density data matrix of fluorescence as a function of time and wavelength. It usually requires an excessive period of time to fully collect such a large matrix, and this may be a severe limitation (especially with proteins and membranes, which may not be stable over many days). Fluorescence decay curves provide good time resolution, but at single wavelengths. The reverse situation prevails for measurement of a few time-resolved emission spectra. The combined method described here can yield sufficient data in a few hours to generate DAS at nanometer resolution for a binary mixture. Recent advances in numerical techniques to correct for instrument "pile-up" saturation (Knutson et al., 1982b) indicate that it should be possible to even further reduce (by 10-fold or more) the time required to obtain DAS at high resolution. While this report has focused on the separation of two or three components, it is clear that the potential exists to discern *several* DAS in a heterogeneous system. The accurate resolution of multiple decay functions (especially among those which are very similar) in a mixture presents the limiting step in these more complex applications.

In summary, DAS can be used to "unmix" several types of heterogeneity in fluorescence spectra, with verifiable accuracy.

Acknowledgments

We thank J. B. A. Ross, R. E. Dale, R. P. DeToma, B. K. Selinger, A. A. Kowalczyk, L. Davenport, E. G. Jablonski, and M. D. Barkley for helpful discussions. We especially thank I. Z. Steinberg for his detailed discussions and encouragement. We are grateful to Linda Hall for her patience with the manuscript and to Nancy Beechem for graphic arts assistance.

References

Abdallah, M. A., Biellman, J. F., Wiget, P., Joppich-Kuhn, R., & Luisi, P. L. (1978) *Eur. J. Biochem. 89*, 397–405.
Ainsworth, S. (1961) *J. Phys. Chem. 65*, 1968–1972.
Badea, M. G., & Brand, L. (1979) *Methods Enzymol. 61*, 378–425.
Bevington, P. R. (1969) *Data Reduction and Error Analysis for the Physical Sciences*, McGraw-Hill, New York.
Blomquist, C. H. (1967) *Arch. Biochem. Biophys. 122*, 24–31.
Brändén, C.-I., Jornvall, H., Eklund, H., & Furugren, B. (1975) *Enzymes, 3rd Ed. 11*, 103–190.
Chen, L. A., Dale, R. E., & Brand, L. (1977) *J. Biol. Chem. 252*, 2163–2169.
DeLuca, M., Brand, L., Cebula, T. A., Seliger, H. H., & Makula, A. F. (1971) *J. Biol. Chem. 246*, 6702–6704.
DeToma, R. P., Easter, J. H., & Brand, L. (1976) *J. Am. Chem. Soc. 98*, 5001–5007.
Easter, J. M., DeToma, R. P., & Brand, L. (1976) *Biophys. J. 16*, 571–583.
Eftink, M. R., & Selvidge, L. A. (1982) *Biochemistry 21*, 117–125.
Eisinger, J. (1969) *Photochem. Photobiol. 9*, 247–258.
Eklund, H., Nordström, B., Zeppenzauer, E., Söderland, G., Ohlsson, I., Boiwe, T., Söderberg, B. O., Tapia, O., Brändén, C.-I., & Åkeson, Å. (1976) *J. Mol. Biol. 102*, 27–59.
Gafni, A., & Brand, L. (1978) *Chem. Phys. Lett. 58*, 346–350.
Gafni, A., Modlin, R. L., & Brand, L. (1975) *Biophys. J. 15*, 263–280.
Gafni, A., Modlin, R. L., & Brand, L. (1976) *J. Phys. Chem. 80*, 898–904.
Halvorson, H. R. (1981) *Biophys. Chem. 14*, 177–184.
Heitz, J., & Brand, L. (1971) *Arch. Biochem. Biophys. 144*, 286–291.
Knutson, J. R., Walbridge, D. G., & Brand, L. (1981) *Abstr. Am. Soc. Photobiol. 9*, 62.
Knutson, J. R., Davenport, L., & Brand, L. (1982a) *Biophys. J. 37*, 203a.
Knutson, J. R., Selinger, B. K., & Brand, L. (1982b) *Abstr. Am. Soc. Photobiol. 10*, 69.

Lakowicz, J. R., & Cherek, H. (1981a) *J. Biochem. Biophys. Methods 5*, 19–35.
Lakowicz, J. R., & Cherek, H. (1981b) *J. Biol. Chem. 256*, 6348–6353.
Laws, W. R., & Shore, J. D. (1978) *J. Biol. Chem. 253*, 8593–8597.
Laws, W. R., & Brand, L. (1979) *J. Phys. Chem. 83*, 795–802.
Meech, S. R., O'Connor, D. V., Roberts, A. J., & Phillips, D. (1981) *Photochem. Photobiol. 33*, 159–172.
Ross, J. B. A., Schmidt, C. J., & Brand, L. (1981) *Biochemistry 20*, 4369–4377.
Vallee, B. L., & Hoch, F. L. (1957) *J. Biol. Chem. 225*, 185–189.
Ware, W. R., Lee, S. K., & Chow, P. (1968) *Chem. Phys. Lett. 2*, 356–358.
Ware, W. R., Lee, S. K., Brant, G. J., & Chow, P. P. (1971) *J. Chem. Phys. 54*, 4729–4737.
Weber, G. (1961) *Nature (London) 190*, 27–29.

Proton and Fluorine Nuclear Magnetic Resonance Spectroscopic Observation of Hemiacetal Formation between *N*-Acyl-*p*-fluorophenylalaninals and α-Chymotrypsin†

David G. Gorenstein* and Dinesh O. Shah

ABSTRACT: Proton nuclear magnetic resonance (NMR) spectroscopy shows that the free aldehyde and not the hydrate of *N*-acetyl-DL-*p*-fluorophenylalaninal binds to α-chymotrypsin. A proton NMR cross-saturation experiment shows that the initial noncovalent complex is in equilibrium with a hemiacetal formed between the aldehyde and the active site serine residue. Fluorine NMR spectra of *N*-acetyl-DL- (and *N*-acetyl-L-) *p*-fluorophenylalaninal in the presence of α-chymotrypsin show separate signals for the hemiacetal complex, the bound aldehyde, the free aldehyde, and the free hydrate. *N*-Benzoyl-DL-*p*-fluorophenylalaninal fluorine NMR signals are also observed for all species except the bound aldehyde form in the presence of α-chymotrypsin. The D and L enantiomers of the hydrate of the *N*-acetyl aldehyde inhibitor give separate fluorine NMR signals, arising from chemical exchange between the L-aldehyde–α-chymotrypsin complex and the free L hydrate. The enzyme-bound inhibitor fluorine signals disappear upon proton decoupling due to a negative nuclear Overhauser effect. Upon gated decoupling of protons, the L hydrate and free aldehyde fluorine signals are reduced in intensity relative to that of the D hydrate signal in the racemate aldehyde complex. This is attributed to a saturation transfer of the heteronuclear nuclear Overhauser effect.

Peptide aldehydes related to substrates have proven to be potent inhibitors of serine proteases (Aoyagi et al., 1969; Kondo et al., 1969; Kawamura et al., 1969; Ito et al., 1972; Thompson, 1973, 1974). Thompson suggested that the tighter binding of the aldehydes derives from stabilization of a hemiacetal tetrahedral adduct formed between the enzyme active site serine and the aldehyde carbonyl. This hemiacetal complex is believed to resemble the transition-state structure in substrate hydrolysis. Enzymes are predicted to bind transition-state structures more tightly than ground-state structures (Pauling, 1946; Wolfenden, 1972; Lienhard, 1972, 1973), and hence, any "transition-state analogue" such as the aldehyde inhibitors of the serine proteases should have a higher affinity for the enzyme than substrate or product analogue structures. Evidence for support of the hemiacetal structure has been indirect, as for example, Lewis & Wolfenden's (1977) secondary deuterium isotope effect on the association of benzamidoacetaldehyde to the cysteine protease papain, which suggests formation of a thiol–hemiacetal.

Gorenstein et al. (1976) had, in fact, shown that simply binding of an aldehyde (cinnamaldehyde) to a serine protease (α-chymotrypsin) was not sufficient evidence of itself to warrant the conclusion of transition-state stabilization in its binding. This proton nuclear magnetic resonance (NMR) study of the cinnamaldehyde binding to α-chymotrypsin (Cht) gave no evidence for the putative hemiacetal–enzyme complex. Similarly Breaux & Bender (1975) in a UV–vis spectroscopic study of substituted cinnamaldehydes binding to Cht could find no evidence in support of the transition state analogue, hemiacetal structure. Lowe & Nurse (1977) introduced an NMR double resonance experiment that provided strong evidence in favor of the hemiacetal structure for the hydrocinnamaldehyde–Cht complex (as originally suggested by Schultz & Cheerva, 1975). In this double resonance experiment the aldehydic proton of the aldehyde in the presence of Cht was cross saturated on proton irradiation in the region expected for the hemiacetal formed with the active site serine. In confirmation of Gorenstein's et al. (1976) earlier conclusion on cinnamaldehyde, no cross-saturation effects were noted with this aldehyde and Cht (Lowe & Nurse, 1977).

In a collaborative experiment, Lowe, Schultz, Gorenstein, and co-workers (Chen et al., 1979) applied proton NMR spectroscopy to the interaction of *N*-benzoyl- and *N*-acetyl-L-phenylalaninals with Cht and dehydroalanine-195–α-chymotrypsin. From line-width changes and cross-saturation effects it was shown that these specific aldehyde transition-state analogues do bind as the hemiacetal to Cht. Proton NMR signals for the hemiacetal structure, however, were never directly observed and were only inferred from the selective

† From the Department of Chemistry, University of Illinois at Chicago, Chicago, Illinois 60680. *Received February 23, 1982.* This work was supported by the National Institutes of Health (GM-17575) and the Alfred P. Sloan Foundation (fellowship to D.G.G.).

0006-2960/82/0421-4679$01.25/0 © 1982 American Chemical Society